Eur Radiol (2017) 27:918–926
DOI 10.1007/s00330-016-4458-4

COMPUTED TOMOGRAPHY

CT spectral imaging for monitoring the therapeutic efficacy of VEGF receptor kinase inhibitor AG-013736 in rabbit VX2 liver tumours

Peijie Lv[1] · Jie Liu[1] · Xiaopeng Yan[1] · Yaru Chai[1] · Yan Chen[1] · Jianbo Gao[1] · Yuanwei Pan[1] · Shuai Li[1] · Hua Guo[1] · Yue Zhou[1]

Received: 23 February 2016 / Revised: 21 April 2016 / Accepted: 30 May 2016 / Published online: 10 June 2016

Abstract

Purpose The aim of this study was to evaluate the value of computed tomography (CT) spectral imaging in assessing the therapeutic efficacy of a vascular endothelial growth factor (VEGF) receptor inhibitor AG-013736 in rabbit VX2 liver tumours.

Methods Twenty-three VX2 liver tumour–bearing rabbits were scanned with CT in spectral imaging mode during the arterial phase (AP) and portal phase (PP). The iodine concentrations(ICs)of tumours normalized to aorta (nICs) at different time points (baseline, 2, 4, 7, 10, and 14 days after treatment) were compared within the treated group (n = 17) as well as between the control (n = 6) and treated groups. Correlations between the tumour size, necrotic fraction (NF), microvessel density (MVD), and nICs were analysed.

Results The change of nICs relative to baseline in the treated group was lower compared to the control group. A greater decrease in the nIC of a tumour at 2 days was positively correlated with a smaller increase in tumour size at 14 days ($P < 0.05$ for both). The tumour nIC values in AP and PP had correlations with MVD (r = 0.71 and 0.52) and NF (r = -0.54 and -0.51) ($P < 0.05$ for all).

Conclusions CT spectral imaging allows for the evaluation and early prediction of tumour response to AG-013736.

Key Points

- *AG-013736 treatment response was evaluated by CT in a rabbit tumour model.*
- *CT spectral imaging allows for the early treatment monitoring of targeted anti-tumour therapies.*
- *Spectral CT findings correlated with vascular changes after anti-tumour therapies.*
- *Spectral CT is a promising method for assessing clinical treatment response.*

Keywords Computed tomography · CT spectral imaging · Vascular targeting agent · Liver tumour · Animal experience

Abbreviations

AP	Arterial phase
PP	Portal phase
IC	Iodine concentration
VTA	Vascular targeting agent
VEGF	Vascular endothelial growth factor
MD	Material decomposition

Introduction

Tumour vessels in tumour angiogenesis are structurally and functionally abnormal, and are essential for tumour growth, progression, and metastasis. The inhibition of tumour vasculature can be a valuable target for cancer therapy. Tumour vascular targeting agents (VTAs) [1, 2] can be classified into either angiogenesis inhibitors [3, 4] such as antiangiogenic drugs, which inhibit new vessel formation by interrupting essential aspects of angiogenesis, or vascular disrupting agents [5], which cause the damage of the previously established

✉ Jianbo Gao
jianbogao0307@163.com

[1] The Department of Radiology, The First Affiliated Hospital of Zhengzhou University, No.1, East Jianshe Road, Zhengzhou, Henan Province, China 450052

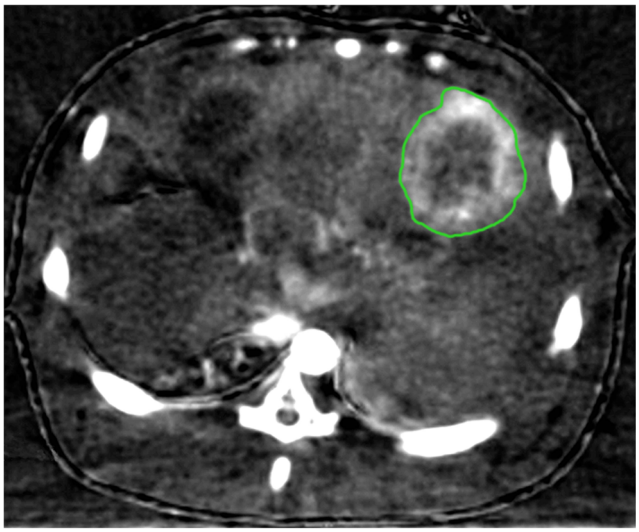

Fig. 1 An axial iodine-based material decomposition image in rabbit shows placement of region of interest around the entire tumour (green outline)

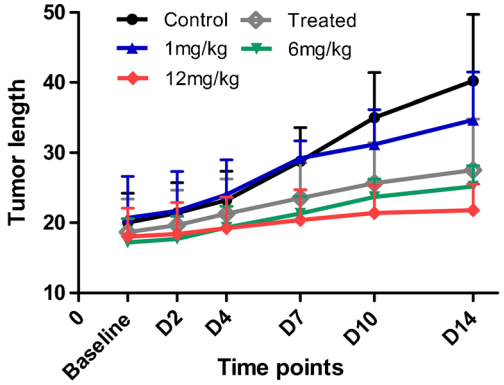

Fig. 2 The tumour longest diameter showed as mean ± standard deviation at different time points, and five to six tumours were included per group. The tumours in the control and treated groups (three different doses of AG-013736: 1 mg/kg bid in group 2, 6 mg/kg bid in group 3, and 12 mg/kg bid in group 4) all grew gradually as a function of days following initiation of treatment, but grew more slowly in the treated group since D7($P < 0.05$)

tumour endothelium and vascular shutdown, subsequently resulting in tumour ischemia and necrosis.

AG-013736 (Axitinib), the small molecule tyrosine kinase inhibitor that targets all known vascular endothelial growth factor (VEGF) receptors, potently inhibits angiogenesis and has single-agent clinical activity in a range of solid tumours [6–8]. The development of novel therapeutic agents targeting angiogenesis is challenging without a validated non-invasive biomarker of an anti-angiogenic effect in humans. A suitable biomarker may increase the probability of detecting a true antitumor effect, as well as predict clinical activity after treatment in a short course. Computed tomography (CT) imaging-based therapy monitoring has gained an important role in oncologic imaging [9–11]. Tumour size change in conventional CT has been widely used to assess antitumor response [11–13]. However, it cannot be relied upon for estimating tumour response to due to its insensitivity or its delayed identification [12, 14]. The use of perfusion CT functional imaging in tumour angiogenesis has also been limited in clinical practice owing to low spatial resolution [15] and poor image quality caused by the low tube voltage [16], posing new demands on CT functional imaging techniques.

Dual-energy spectral CT using a single-detector, single-source with rapid-kV-switching between two peak voltage settings(140 kVp and 80 kVp), allows the reconstruction of accurate material-decomposition (MD) images (e.g., water- and iodine-based MD images) for iodine concentration (in milligrams per millilitre) derivation. Multiple studies have demonstrated the validity of iodine concentration quantification in material differentiation, material identification and tumour response after radiotherapy or chemotherapy [17–21]. CT spectral imaging parameters might be useful in repeated monitoring of the microenvironmental change of tumours after administration of antiangiogenic agents, because antiangiogenic agents would affect the tumour vasculature and result in necrosis of the tumour, causing the change of iodine concentration in tumours after iodinated contrast agent administration. However, to date, there are few studies dealing with the use of spectral CT for evaluating therapeutic response of AG-013736.

The current study aims to assess the capacity of using CT spectral imaging parameters to evaluate the therapeutic response of AG-013736 in inhibiting VX2 liver tumours in rabbits.

Materials and methods

Animal model

The ethics review committee of the life sciences in our institution approved the animal experiments. New Zealand male rabbits (Experimental Animal Center of Zhengzhou University) weighing 2.5–3.5 kg were anesthetized with intramuscular injection of xylazine hydrochloride (Shengda Co., Jilin, China) at a dose of 0.2 ml/kg body weight. The rabbit VX2 tumour model was used because of its hepatic artery blood supply [22] and biological progression [23] similar to that of human hepatocellular carcinoma. The intramuscular growth of VX2 tumour-bearing rabbit was harvested under the same anaesthesia when tumour portions grew approximately 4 cm^3 in volume. Chunks of the tumour were minced into 2.0 mm^3 cubes and implanted into the left liver lobes through a 17 gauge catheter under CT (Discovery CT590 RT, GE Healthcare, Milwaukee, Wisconsin, USA) guidance (Y.W.P and S.L), inducing liver solitary tumours in 14 days with a diameter of 1–2 centimetres in the longest dimension,

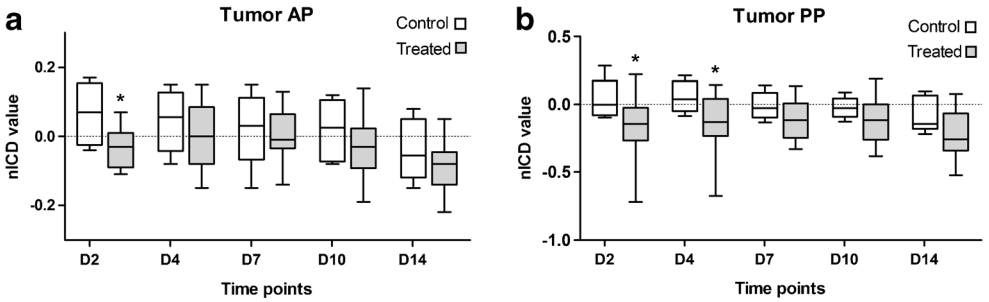

Fig. 3 Box-and-whisker plots (box: 25 %, 75 %; centreline: medium; whisker: min, max) show normalized iodine concentration differences (nICD) values of the tumours between the given time and baseline during the AP (**a**) and PP (**b**). $P < 0.05$ (*) indicates a statistically significant difference between the control and treated groups by using the Mann-Whitney test

which would have relatively high vascularity and not be too small for imaging [24].

AG-013736 preparation and study protocol

AG-013736 (Selleckchem.LLC, Texas, USA), a receptor kinase inhibitor of all known VEGF receptors, was prepared in a 0.5 % carboxymethyl cellulose suspension vehicle, and given orally by gavage at a dose of 1, 6 or 12 mg/kg (twice daily in the fasted state). The dose was selected based on the conversion of effective dose for mice studies (30 mg/kg twice daily) [25, 26] and the maximum tolerated dose (10 mg twice daily) of AG-013736 defined during the phase II trial in patients with advanced hepatocellular carcinoma [27].

Twenty-nine qualified tumour-carrying rabbits were randomly assigned by means of random number lists into the control group (n = 6; group 1) and AG-013736–treated groups at different dosage regimens of 1 mg/kg (n = 8; group 2), 6 mg/kg (n = 9; group 3), and 12 mg/kg (n = 6; group 4). Spectral CT scan were performed in all rabbits before (baseline) and at 2 days, 4 days, 7 days,10 days and 14 days after AG-013736 treatment. During the 14-day follow-up, six rabbits (two in group 2, three in group 3 and one in group 4) in the treated group died during the experimental period, which may be related to the factors such as laparotomy procedure, repeated anaesthesia or imaging studies, and the toxicity of the agent. Finally, six rabbits in the control group (group 1) and 17 in the treated group (six each in groups 2 and 3, five in group 4) were included in this study.

Table 1 Comparisons of normalized iodine concentration difference (nICD) between the control group and group 4 (AG-013736 of 12 mg/kg bid) at different time points

Parameter	Group		*P* value
	Control group	Group 4	
nICD in AP			
2 Days	0.067 ± 0.086	-0.065 ± 0.037	0.015
4 Days	0.045 ± 0.087	-0.028 ± 0.011	0.240
7 Days	0.020 ± 0. 112	-0.068 ± 0.080	0.310
10 Days	0.020 ± 0. 083	-0.084 ± 0.028	0.041
14 Days	-0.042 ± 0.092	-0.092 ± 0.025	0.485
nICD in PP			
2 Days	0.041 ± 0.148	-0.222 ± 0.081	0.004
4 Days	0.054 ± 0.122	-0.201 ± 0.104	0.004
7 Days	-0.011 ± 0.100	-0.197 ± 0.184	0.175
10 Days	-0.039 ± 0.250	-0.292 ± 0.100	0.044
14 Days	-0.086 ± 0.131	-0.271 ± 0.109	0.026

Data are means ± standard deviations. With the Mann-Whitney test , a significance threshold of $P < 0.05$ was used.

CT scanning

Triple-phase spectral CT scans (i.e. unenhanced and two-phase contrast enhanced CT examinations) on all animals were performed on a Discovery CT750HD system (GE Healthcare, Milwaukee, Wisconsin, USA). Under the same anaesthesia, the rabbits were fixed on a board in supine position with abdominal bandage to further reduce the respiratory movement.

Two-phase contrast-enhanced CT images covering the whole liver were acquired in the spectral imaging mode (Gemstone Spectral Imaging (GSI) protocol 32, GSI-32) with a single tube, rapid dual kVp (80 kVp and 140 kVp) switching technique. Other parameters were as follows: collimation, 64 × 0.625 mm; tube current, 375 mA; rotation speed, 0.6 second; helical pitch, 0.984:1. Animals were injected with 5.0 ml of non-ionic contrast medium (Ioversol Injection, Optiray 320; Jiangsu Hengrui Medicine Co., China) through auricular venous access at a rate of 1 mL/s followed by 10 mL of saline administered at the same rate using a power injector (Envision CT injector, Medrad, Georgia, United States). The arterial and portal venous phase imaging began 15 s and 35 s after the administration of contrast agent.

The spectral CT images were reconstructed by using projection-based material decomposition software and a standard reconstruction kernel with slice thickness and reconstruction interval of 1.25 mm. Water- and iodine-based MD images

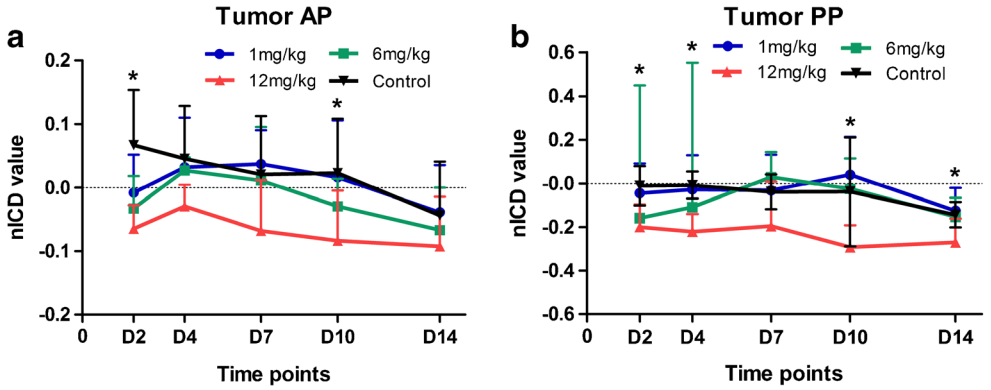

Fig. 4 Normalized iodine concentration differences (nICD) values of the tumours in the control and treated groups during AP (**a**) and PP (**b**) as a function of days following initiation of treatment. Comparisons between control group and treated groups with three different doses of AG-013736 (1 mg/kg bid in group 2, 6 mg/kg bid in group 3, and 12 mg/kg bid in group 4) at each time point were performed by using the Mann-Whitney test (* = $P < 0.05$). During AP, tumours nICDs in group 4 at day 2 and day 10 were significantly lower than in the control group. During PP, tumour nICDs in group 4 at each time point except at day 7 decreased significantly compared to the control group

as basis material pairs were reconstructed from the single spectral CT acquisition for analysis.

Image analysis

Two radiologists (H.G and J.B.G) with 18-32 years' experience in abdominal imaging performed the quantitative measurements in consensus for analyzing the iodine-based MD images by using the GSI viewer software on a commercially available workstation (Advantage Windows, version 4.4; GE Healthcare, Wisconsin, USA). The change in tumour size was defined at the longest dimension measured on the iodine-based MD images to determine the effect of tumour treatment. Percentage change in tumour size (ΔTS) [12] on all rabbits between baseline and 14-day follow-up was calculated as following: $\Delta TS = (LD_{14days} - LD_{baseline})/LD_{baseline} * 100\ \%$, where LD is the longest dimension of the tumour.

At each time point, an iodine concentration (IC) of the tumour was measured on the iodine-based MD image by using an operator-defined region of interest (ROI) (mean value 206 mm^2, range 102– 409 mm^2) around the entire tumour [13, 28] (Fig. 1). In order to minimize variations between rabbits, the IC of tumour was normalized to the iodine concentration in the aorta (IC_{aorta}) to derive a normalized iodine concentration (nIC): $nIC = IC_{tumour}/IC_{aorta}$. The difference for the normalized iodine concentration (nICD) between a given time and baseline were calculated as follows:

Table 2 Comparisons of normalized iodine concentration (nIC) for the tumour between different time points in the treated Group (n = 17)

Parameter	Measurement	*P* value				
		2 Days	4 Days	7 Days	10 Days	14 Days
nIC in AP						
Baseline	0.148 (0.032-0.407)	<0.001	0.032	0.445	0.011	<0.001
2 Days	0.081 (0.016-0.164)		0.041	0.056	0.275	0.251
4 Days	0.113 (0.048-0.205)			0.627	0.745	0.004
7 Days	0.129 (0.026-0.289)				0.366	0.001
10 Days	0.103 (0.044-0.255)					0.014
14 Days	0.074 (0.020-0.158)					
nIC in PP						
Baseline	0.491 (0.157-2.219)	0.004	0.035	0.100	0.264	0.001
2 Days	0.293 (0.124-0.467)		0.300	0.416	0.943	0.029
4 Days	0.326 (0.167-0.519)			0.808	0.271	0.003
7 Days	0.329 (0.123-0.488)				0.577	0.002
10 Days	0.315 (0.141-0.685)					0.005
14 Days	0.257 (0.155-0.421)					

Data are means, with ranges in parentheses. With the Wilcoxon signed rank test, a significance threshold of $P < 0.0042$ was used

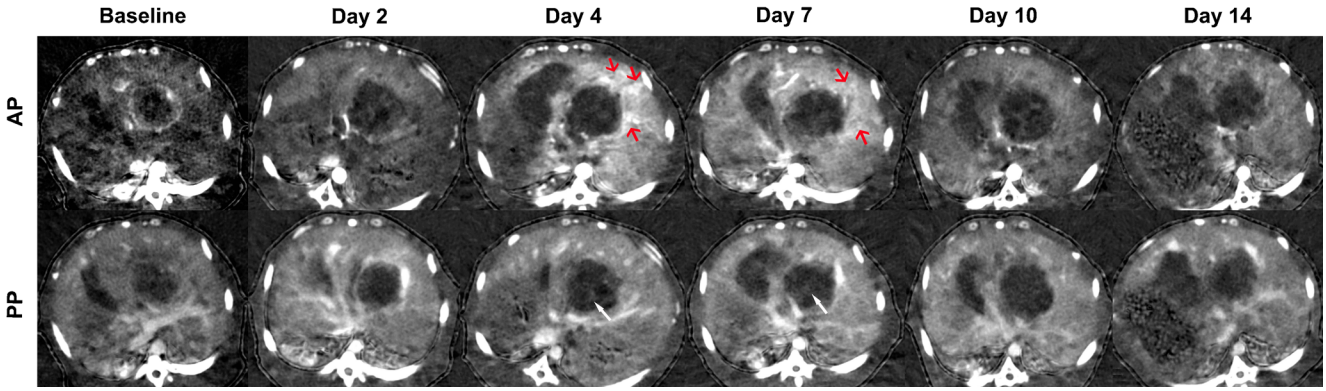

Fig. 5 Iodine–based material decomposition images at different time points in group 4 (AG-013736 treated with 12 mg/kg bid) during AP and PP. 2 days after treatment, the iodine concentration of tumour is sharply decreased, but obvious hyperintense peritumoral rims (red arrow) in AP and slightly hyperintense centres (white arrow) relative to that of day 2 in PP were noticed at 4 days and 7 days .The iodine concentration gradual decreases from 10 days to 14 days

$nICD = nIC_{given\ time} - nIC_{baseline}$. For all measurements, an average of three separate ROIs was obtained to ensure consistency and the copy-and-paste function was applied to make sure the ROIs were at the same place in the two phases.

Histological analysis

The rabbits were sacrificed immediately after spectral CT scan by the intravenous injection of 10 ml of 10 % kalium chloratum while they were deeply anesthetized. After fixation in 10 % buffered formalin, the tumour specimens excised from the rabbit livers were sliced at approximately 1 mm intervals in the transverse plane to match the CT images. Hematoxylin-eosin (HE) staining at 3 μm section was performed to evaluate the necrotic fraction (NF) of the tumour by using the following formula: $NF = Area_{necrosis} / Area_{totaltumor}$ [12]. The blood vessel marker CD31 expressions were detected to analyze the microvessel density (MVD) of the tumours by using immunohistochemical methods for the specific endothelial antigen CD31. To obtain the MVD of the tumour, hot spots (highest vascular density area within the lesions) were identified at low magnification (×100), and the three areas with highest CD31-stained vessels were counted at high magnification (×200; 0.458 mm^2/field) to obtain the mean value.

Table 3 Correlation between histological features and normalized iodine concentration (nIC) of the tumour at 14–day follow up

	MVD		NF	
Parameter	r	*P* value	r	*P* value
nIC in AP	0.71	0.001	-0.54	0.027
nIC in PP	0.52	0.033	-0.51	0.037

All *P* values were calculated with the Spearman rank correlation test, with $P < 0.05$ indicating a statistically significant difference

Statistical analysis

All statistical analyses were performed by using SAS (SAS, version 9.1.3; SAS Institute, Cary, NC). To evaluate the reproducibility of CT spectral imaging parameters, tumour nIC values at baseline in the control group (n = 6) were compared with the nIC values measured again at 6 hours later in the arterial phase (AP) and portal phase (PP) to calculate the corresponding coefficients of variation (CVs) within rabbits (good reproducibility, CVs of 10 % or less; moderate, 10 %–25 %; poor, 25 % or greater) [29]. Considering the skewed distribution of data probably because of the small number of samples, the Mann-Whitney test or the Kruskal-Wallis test with post-hoc comparison was used to compare the tumour size change and CT spectral imaging values between the control and treated groups or among the treated groups with different dosage regimens. Serial changes in nICs of the tumours in the treated group (n =17) at different time points were evaluated by using the Friedman test, with post-hoc Wilcoxon signed rank test used for further comparisons in cases of statistical significance. The correlation between nICDs and the tumour size changes at 14 days, and the correlation between nICs at 14 days and corresponding histological features such as NF and MVD were assessed using Spearman rank correlation test due to the skewed or ordinal distribution of data. All statistical analyses were performed with $P < 0.05$ indicating a statistically significant difference. For the case of the post-hoc Wilcoxon signed rank test (12 paired comparisons at six points),

$P < 0.0042$ (0.05/12) was considered to indicate significance for a Bonferroni correction.

Results

Tumour growth

The Rabbits carrying VX2 tumours were first treated with 1, 6, or 12 mg/kg/bid AG-013736 to define a dose that would not stop but slow tumour growth (Fig. 2).The percentage increase in the tumour size was significantly smaller in the treated group (median, 58.62 %) than that in the control group (median, 100.1 %) ($P = 0.024$). This size increase of the tumour in the treated groups tended to be smaller with higher dosages (median, 75.73 %, 65.69 %, and 42.85 % in group 2, 3, and 4, respectively), with statistically significant difference between group 4 and the control group ($P = 0.004$). However, there was no statistically significant difference among the three kinds of dosage regimens ($P = 0.247$).

Reproducibility of CT spectral imaging parameters

In the control group, nICs of the tumours demonstrated good reproducibility, with within-subject CVs of 6.10 % and 8.56 % in AP and PP respectively.

Comparison between the control and treated groups

In general, the differences of the normalized iodine concentrations (nICDs) of the tumours relative to baseline for each group at each time point in AP and PP were lower in the treated group as compared with the control group (Fig. 3). nICDs of the tumours were significantly lower in the treated group than in the control group at 2 days (-0.031 ± 0.055 vs. 0.067 ± 0.086, $P = 0.015$) in AP; and at 2 days (-0.166 ± 0.239 vs. 0.041 ± 0.148, $P = 0.032$) and 4 days (-0.144 ± 0.240 vs. 0.054 ± 0.122, $P = 0.020$) in PP after treatment.

All parameters between the subgroups 2 and 3 (treated with 1 mg/kg and 6 mg/kg dose of AG-013736, respectively) and the control group (Table 1 and Fig. 4) showed no statistically significant difference at any follow-up time points. Compared with the control group, group 4 showed significantly lower nICDs at 2 days ($P = 0.015$ and 0.004 for AP and PP respectively) , almost similar results at 4 days and 7 days, but almost lower values at 10 days and similar (AP) or lower values (PP) at 14 days after treatment. For all nICDs of the tumours at any follow-up time points, there were no statistically significant differences among the three subgroups in the treated group.

Serial measurements in the treated group

Results for serial measurements of nICs of the tumours in the treated group are summarized in Table 2. Compared with the baseline, nICs in the treated group at 2-day follow-up decreased significantly ($P < 0.0042$), but recovered at 4-day and 7-day follow-ups with no significant differences, whereas nICs decreased slightly at 10 days and significantly at 14 days after treatment ($P < 0.001$ and 0.001 for AP and PP respectively) (Fig. 5). nICs significantly decreased at 14 days as compared with 4 days and 7 days (All P values < 0.0042).

Prediction of tumour response

There was statistically significant positive correlation with tumour response for nICDs of the tumours at 2-day follow-up in both AP ($r = 0.69$, $P = 0.002$) and PP ($r = 0.64$, $P = 0.006$) after treatment, which meant that a greater increase in nICD at 2 days would predict a smaller increase in tumour size at 14 days.

Histological analysis

The correlation between nICs of the tumours at 14-day follow-up and corresponding histological features, including NF and MVD were showed in Table 3. NF was significantly correlated with nICs of tumours negatively in both AP and PP. MVD showed positive correlation with nICs of the tumours in both AP and PP.

Discussion

AG-013736 has been shown to inhibit angiogenesis, vascular permeability, blood flow and antimetastatic activity in previous nonclinical and clinical studies [6, 7, 30]. In this study, AG-013736 was administered in rabbits with VX2 liver tumours, which are most commonly used large animal model in imitating primary or secondary liver cancers in humans [13, 31, 32]. A number of studies about the effect of AG-013736 on breast cancer, prostate cancer, neuroblastoma and cholangiocarcinoma have been tested previously in rat and mouse models [7, 25, 33]. This is the first time the anti-angiogenic agent of AG-013736 has been tested for antitumor efficacy in this model.

In this study, the change of tumour size was evaluated by using the longest dimension of the tumour instead of tumour volume, based on the methodologies of previous literatures [12, 34–36] and the fact that our all tumours showed interval growth indicating progressive disease. The results on tumour size demonstrated that tumour growth was significantly suppressed by AG-013736 compared with the control, tended to be smaller with higher dosages, similar to the results of Liu G

et al. that the effect of AG-013736 is dose dependent [6]. The ability of quantitative analysis for CT spectral imaging parameters in our study has been proved to be feasible in depicting the serial changes after administration of AG-013736 in a rabbit VX2 liver tumour model, with good reproducibility.

CT with energy information, in particular spectral CT, extends the capabilities of conventional CT. It provides the material-decomposition basis pair of water and iodine in medical diagnostic imaging for quantification [20, 37] in elemental and molecular composition and contrast materials based on their attenuation properties [38]. The quantitative IC in the tumour derived from the iodine-based MD image is an indication of its blood flow [19, 39], depending on the amount of iodinated contrast agent administration. The quantitative measurements obtained in this study showed that nICDs of the treated group were lower as compared with the control group, although not statistically significant in all time points and all parameters. Interestingly, in the treated group, nICs of the tumours decreased at 2 days, recovered at 4 days and 7 days, and further decreased from 10 days to 14 days after the administration of AG-013736. This different responses as function of time after treatment may be explained by the intrinsic mechanism of VEGF inhibitor. It can selectively prune the chaotic and inefficient vasculature commonly found in tumours and improved vasculature by reducing vessel counts and increased coverage of pericytes [40], resulting in the reduction of blood flow to the tumours, which would be followed by ischemic changes such as cellular edema and intratumoral necrosis [12]. However, the peripheral viable tumour usually survives and regrows, appearing to be weaker than the centre of the tumour [13] in the treatment response, reflected by the serial changes of iodine concentrations in the peripheral and central regions of the tumour in our study, similar to other studies [12, 13] about the therapeutic efficacy of VTAs in rabbit VX2 liver tumours. But further repeated drug administration at time intervals have been demonstrated effective in improving therapeutic effects by our and other studies [41].

This study showed that relative changes of iodine concentration in tumours had the potential to predict favourable tumour response after AG-013736 treatment. nICDs of the tumours at 2 days in both AP and PP after treatment showed a statistically significant correlation with the final changes in tumour sizes ($P = 0.002$ and $P = 0.006$, respectively). Consistent with this result, Liu G et al. [6] utilized magnetic resonance imaging to study pharmacodynamic response in AG-013736-treated patients with advanced solid tumours and found day 2 vascular response seemed to be a useful indicator of drug pharmacology. It should be noted that tumour size of VX2 tumours in the treated group grow slowly but progressively, indicating that AG-013736 s are not expected to reduce tumour size, consistent with other studies [6, 25, 42]. The ability of nICDs in reflecting the angiogenesis of the tumour can be explained by the positively correlation between nICs of the tumours and MVD. An increase in nICDs at 4 days after treatment can also be explained by the increase in intratumoral necrosis, considering the significant correlation between nICs and NF at 14 days.

For the assessment of tumour response, there have been few studies evaluating the usefulness of CT spectral imaging. Although Tang L et al. [18] and Hu S et al. [19] have demonstrated the value of spectral CT in evaluating the therapeutic effect of neoadjuvant chemotherapy on gastric carcinomas and ^{125}I interstitial brachytherapy on pancreatic carcinoma, the potential role of CT spectral imaging parameters as early predictors of tumour response after VTA treatments has not been previously well established in the literature. Dual-source dual-energy CT (DECT) has also been demonstrated to be effective in early prediction of tumour response in human study of Meyer M et al. [43], however, this study has used the first available DECT scan instead of prior treatment similar to our study as baseline evaluation, which may lead to a long term evaluation bias. In contrast to the relatively short period of 4 days in the animal study of Knobloch G et al. [44] to assess the early regorafenib treatment effects, the evaluation of AG-013736 treatment in our study was performed during the relatively long period of 14 day so that therapy-related changes in the tumour microvasculature and tumour size could be performed. The study of Lee SH et al. [45] has assessed the value of iodine maps in the evaluation of therapeutic response to radiofrequency ablation (RFA) for hepatic tumours but without evaluating it as early predictors of tumour response.

The present study did have limitations. First, we didn't perform a power analysis in the study, as no prior data existed and assumed that five or more rabbits per group would be sufficient for this animal study. Therefore larger prospective investigations are needed to confirm our findings. Second, the correlation of the CT spectral imaging parameters with histological features at each time point were not evaluated except at 14 days after the treatment, which would not explain the early changes of histological features. Third, the accuracy of quantitative evaluation on VTAs with CT spectral imaging was not validated by other imaging modalities such as perfusion CT, Doppler ultrasound and dynamic contrast-enhanced MR imaging. These shortcomings will be addressed in our future research.

In conclusion, the therapeutic effects of AG-013736 in inhibiting VX2 liver tumours in rabbits can be noninvasively and quantitatively monitored with CT spectral imaging parameters. The day 2 vascular response measured using nICDs from material decomposition images in spectral CT can be used as suitable markers for the early prediction of tumour response.

Acknowledgments The scientific guarantor of this publication is Peijie Lv. The authors of this manuscript declare no relationships with any

companies, whose products or services may be related to the subject matter of the article. The authors wish to thank Yun Shen, Jianying Li, and Ying Guo from GE Healthcare for their technical supports. This study has received funding by National Natural Science Foundation of China (Grant No. 81301220 to P. J. L.) and Medical scientific and technological project in Henan Province (Grant No. 201403016 to P. J. L.). No complex statistical methods were necessary for this paper. Institutional Review Board approval was obtained. Written informed consent was not required for this study because the study was only on animals. Approval from the institutional animal care committee was obtained. No study subjects or cohorts have been previously reported. Methodology: prospective, experimental, performed at one institution.

References

1. McKeage MJ, Baguley BC (2010) Disrupting established tumor blood vessels: an emerging therapeutic strategy for cancer. Cancer 116:1859–1872
2. Salmon BA, Salmon HW, Siemann DW (2007) Monitoring the treatment efficacy of the vascular disrupting agent CA4P. Eur J Cancer 43:1622–1629
3. Shojaei F (2012) Anti-angiogenesis therapy in cancer: current challenges and future perspectives. Cancer Lett 320:130–137
4. Eichten A, Adler AP, Cooper B et al (2013) Rapid decrease in tumor perfusion following VEGF blockade predicts long-term tumor growth inhibition in preclinical tumor models. Angiogenesis 16:429–441
5. Sersa G, Jarm T, Kotnik T et al (2008) Vascular disrupting action of electroporation and electrochemotherapy with bleomycin in murine sarcoma. Br J Cancer 98:388–398
6. Liu G, Rugo HS, Wilding G et al (2005) Dynamic contrast-enhanced magnetic resonance imaging as a pharmacodynamic measure of response after acute dosing of AG-013736, an oral angiogenesis inhibitor, in patients with advanced solid tumors: results from a phase I study. J Clin Oncol 23:5464–5473
7. Wilmes LJ, Pallavicini MG, Fleming LM et al (2007) AG-013736, a novel inhibitor of VEGF receptor tyrosine kinases, inhibits breast cancer growth and decreases vascular permeability as detected by dynamic contrast-enhanced magnetic resonance imaging. Magn Reson Imaging 25:319–327
8. Lu L, Saha D, Martuza RL, Rabkin SD, Wakimoto H (2015) Single agent efficacy of the VEGFR kinase inhibitor axitinib in preclinical models of glioblastoma. J Neurooncol 121:91–100
9. Yang HF, Du Y, Ni JX et al (2010) Perfusion computed tomography evaluation of angiogenesis in liver cancer. Eur Radiol 20:1424–1430
10. Ehling J, Lammers T, Kiessling F (2013) Non-invasive imaging for studying anti-angiogenic therapy effects. Thromb Haemost 109:375–390
11. Smith AD, Lieber ML, Shah SN (2010) Assessing tumor response and detecting recurrence in metastatic renal cell carcinoma on targeted therapy: importance of size and attenuation on contrast-enhanced CT. AJR Am J Roentgenol 194:157–165
12. Joo I, Lee JM, Han JK, Choi BI (2014) Intravoxel incoherent motion diffusion-weighted MR imaging for monitoring the therapeutic efficacy of the vascular disrupting agent CKD-516 in rabbit VX2 liver tumors. Radiology 272:417–426
13. Shao H, Ni Y, Zhang J et al (2013) Dynamic contrast-enhanced and diffusion-weighted magnetic resonance imaging noninvasive evaluation of vascular disrupting treatment on rabbit liver tumors. PLoS ONE 8, e82649
14. Wang J, Wu N, Cham MD, Song Y (2009) Tumor response in patients with advanced non-small cell lung cancer: perfusion CT evaluation of chemotherapy and radiation therapy. AJR Am J Roentgenol 193:1090–1096
15. Jain R, Ellika SK, Scarpace L et al (2008) Quantitative estimation of permeability surface-area product in astroglial brain tumors using perfusion CT and correlation with histopathologic grade. AJNR Am J Neuroradiol 29:694–700
16. Kim KW, Lee JM, Kim JH et al (2011) CT color mapping of the arterial enhancement fraction of VX2 carcinoma implanted in rabbit liver: comparison with perfusion CT. AJR Am J Roentgenol 196:102–108
17. Wu HW, Cheng JJ, Li JY, Yin Y, Hua J, Xu JR (2012) Pulmonary embolism detection and characterization through quantitative iodine-based material decomposition images with spectral computed tomography imaging. Investig Radiol 47:85–91
18. Tang L, Li ZY, Li ZW et al (2015) Evaluating the response of gastric carcinomas to neoadjuvant chemotherapy using iodine concentration on spectral CT: a comparison with pathological regression. Clin Radiol 70:1198–1204
19. Hu S, Huang W, Chen Y et al (2014) Spectral CT evaluation of interstitial brachytherapy in pancreatic carcinoma xenografts: preliminary animal experience. Eur Radiol 24:2167–2173
20. Lv P, Lin XZ, Li J, Li W, Chen K (2011) Differentiation of small hepatic hemangioma from small hepatocellular carcinoma: recently introduced spectral CT method. Radiology 259:720–729
21. Liu X, Ouyang D, Li H et al (2014) Papillary thyroid cancer: dual-energy spectral CT quantitative parameters for preoperative diagnosis of metastasis to the cervical lymph nodes. Radiology 275:167–176
22. Ramirez LH, Julieron M, Bonnay M et al (1995) Stimulation of tumor growth in vitro and in vivo by suramin on the VX2 model. Invest New Drugs 13:51–53
23. Wang Z, Yang G, Nie P, Fu J, Wang X, Liu D (2013) Dynamical observation on biological progression of VX2 liver tumors to identify the optimal time for intervention in animal models. PLoS ONE 8, e74327
24. Wu H, Exner AA, Shi H, Bear J, Haaga JR (2009) Dynamic evolutionary changes in blood flow measured by MDCT in a hepatic VX2 tumor implant over an extended 28-day growth period: time-density curve analysis. Acad Radiol 16:1483–1492
25. Rossler J, Monnet Y, Farace F et al (2011) The selective VEGFR1-3 inhibitor axitinib (AG-013736) shows antitumor activity in human neuroblastoma xenografts. Int J Cancer 128:2748–2758
26. Takahashi H, Ojima H, Shimizu H, Furuse J, Furukawa H, Shibata T (2014) Axitinib (AG-013736), an oral specific VEGFR TKI, shows potential therapeutic utility against cholangiocarcinoma. Jpn J Clin Oncol 44:570–578
27. McNamara MG, Le LW, Horgan AM et al (2015) A phase II trial of second-line axitinib following prior antiangiogenic therapy in advanced hepatocellular carcinoma. Cancer 121:1620–1627
28. Wang D, Bangash AK, Rhee TK et al (2007) Liver tumors: monitoring embolization in rabbits with VX2 tumors–transcatheter intraarterial first-pass perfusion MR imaging. Radiology 245:130–139
29. Iellamo F, Legramante JM, Raimondi G, Castrucci F, Massaro M, Peruzzi G (1996) Evaluation of reproducibility of spontaneous baroreflex sensitivity at rest and during laboratory tests. J Hypertens 14:1099–1104
30. Rugo HS, Herbst RS, Liu G et al (2005) Phase I trial of the oral antiangiogenesis agent AG-013736 in patients with advanced solid tumors: pharmacokinetic and clinical results. J Clin Oncol 23:5474–5483
31. Guo Y, Zhang Y, Jin N et al (2012) Electroporation-mediated transcatheter arterial chemoembolization in the rabbit VX2 liver tumor model. Investig Radiol 47:116–120
32. Wijlemans JW, Deckers R, van den Bosch MA et al (2013) Evolution of the ablation region after magnetic resonance-guided

high-intensity focused ultrasound ablation in a Vx2 tumor model. Investig Radiol 48:381–386
33. Ma J, Waxman DJ (2009) Dominant effect of antiangiogenesis in combination therapy involving cyclophosphamide and axitinib. Clin Cancer Res 15:578–588
34. Birchard KR, Hoang JK, Herndon JE, Patz EF (2009) Early changes in tumor size in patients treated for advanced stage nonsmall cell lung cancer do not correlate with survival. Cancer 115:581–586
35. Gayed I, Vu T, Iyer R et al (2004) The role of 18F-FDG PET in staging and early prediction of response to therapy of recurrent gastrointestinal stromal tumors. J Nucl Med 45:17–21
36. de Baère T, Palussière J, Aupérin A et al (2006) Midterm local efficacy and survival after radiofrequency ablation of lung tumors with minimum follow-up of 1 year: prospective evaluation. Radiology 240:587–596
37. De Cecco CN, Darnell A, Rengo M et al (2012) Dual-energy CT: oncologic applications. AJR Am J Roentgenol 199:S98–S105
38. Feuerlein S, Heye TJ, Bashir MR, Boll DT (2012) Iodine quantification using dual-energy multidetector computed tomography imaging: phantom study assessing the impact of iterative reconstruction schemes and patient habitus on accuracy. Investig Radiol 47:656–661
39. Thaiss WM, Haberland U, Kaufmann S et al (2015) Iodine concentration as a perfusion surrogate marker in oncology: further elucidation of the underlying mechanisms using Volume Perfusion CT with 80 kVp. Eur Radiol
40. Fenton BM, Paoni SF (2007) The addition of AG-013736 to fractionated radiation improves tumor response without functionally normalizing the tumor vasculature. Cancer Res 67:9921–9928
41. Thoeny HC, De Keyzer F, Chen F et al (2005) Diffusion-weighted magnetic resonance imaging allows noninvasive in vivo monitoring of the effects of combretastatin a-4 phosphate after repeated administration. Neoplasia 7:779–787
42. Hu-Lowe DD, Zou HY, Grazzini ML et al (2008) Nonclinical antiangiogenesis and antitumor activities of axitinib (AG-013736), an oral, potent, and selective inhibitor of vascular endothelial growth factor receptor tyrosine kinases 1, 2, 3. Clin Cancer Res 14:7272–7283
43. Meyer M, Hohenberger P, Apfaltrer P et al (2013) CT-based response assessment of advanced gastrointestinal stromal tumor: dual energy CT provides a more predictive imaging biomarker of clinical benefit than RECIST or Choi criteria. Eur J Radiol 82:923–928
44. Knobloch G, Jost G, Huppertz A, Hamm B, Pietsch H (2014) Dual-energy computed tomography for the assessment of early treatment effects of regorafenib in a preclinical tumor model: comparison with dynamic contrast-enhanced CT and conventional contrast-enhanced single-energy CT. Eur Radiol 24:1896–1905
45. Lee SH, Lee JM, Kim KW et al (2011) Dual-energy computed tomography to assess tumor response to hepatic radiofrequency ablation: potential diagnostic value of virtual noncontrast images and iodine maps. Investig Radiol 46:77–84